Waste and Biomass Valorization (2024) 15:1005–1018
https://doi.org/10.1007/s12649-023-02208-2

ORIGINAL PAPER

Binder-Free Textile PAN-Based Electrodes for Aqueous and Glycerol-Based Electrochemical Supercapacitors

Ingrid Ariani Belineli Barbosa[1] · Jossano Saldanha Marcuzzo[2] · Ivana Conte Cosentino[1] · Rubens Nunes de Faria Jr[1]

Received: 1 February 2023 / Accepted: 8 June 2023 / Published online: 4 July 2023

Abstract

Amidst different types of energy storage systems, electrochemical supercapacitors have received considerable attention as they close the gap between electrolytic capacitors and batteries. This work addresses electric double-layer capacitors (EDLCs), a type of electrochemical supercapacitor, and has been divided into two parts. In the former, the synthesis and characterization of activated carbon fiber-felt (ACFF) electrodes, derived from textile PAN-based fiber, have been provided. In the latter, the electrochemical characterization of EDLCs in potassium hydroxide solutions (aqueous electrolytes) and in potassium hydroxide-glycerol hybrid electrolytes (glycerol-based electrolytes) have been investigated. The synthesis of ACFF electrodes via two-step oxidation, carbonization, and physical activation resulted in low-cost and binder-free electrodes containing 87% of the total volume of pores as micropores (maximum pore width of 3 nm) and a high specific surface area of 1875 $m^2\ g^{-1}$. Electrochemical impedance spectroscopy, cyclic voltammetry, and galvanostatic charge–discharge techniques were carried out in a symmetric two-electrode setup at room temperature. The results showed that ACFF electrodes are suitable for aqueous electrolytes, particularly 2 M KOH, and KOH:GLY (3:1), a glycerol-based electrolyte. Although KOH:GLY (3:1) exhibited high electrolyte resistance ($34 \pm 3\ \Omega$), this hybrid green-electrolyte supports a potential window that is twice greater than that of aqueous electrolytes. In addition, glycerol, commonly called glycerin, is a by-product of FAME (fatty acid methyl ester) biodiesel, which is the major source of glycerol. Glycerol-based electrolytes are promising green electrolytes for EDLCs. Therefore, it is necessary to decrease its viscosity and resistance.

Graphical Abstract

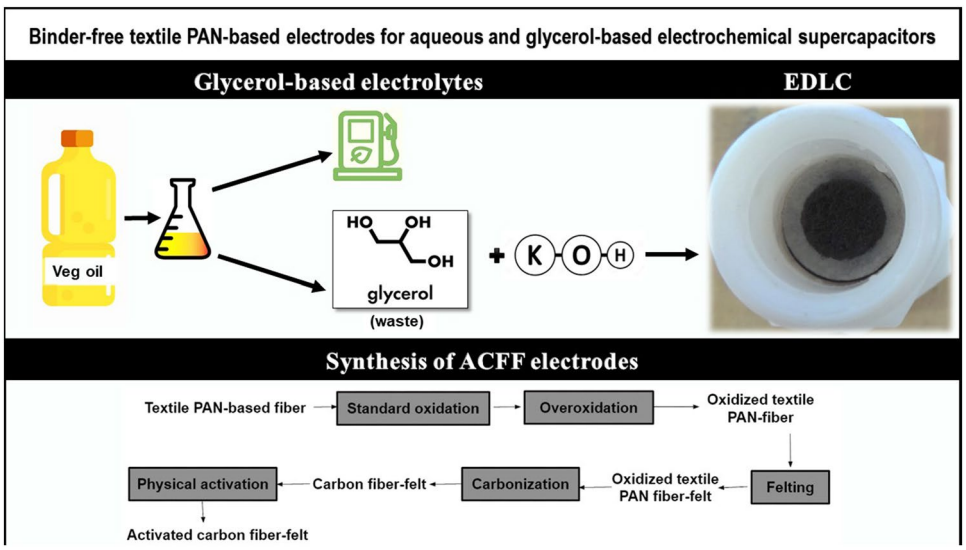

Keywords Supercapacitors · EDLC · PAN fibers · Glycerol · KOH · Green electrolytes

Extended author information available on the last page of the article

Novelty Statement

Among the different types of energy storage systems, electrochemical supercapacitors (SCs) have drawn a lot of attention as they bridge the gap between electrolytic capacitors and batteries. Organic electrolytes, which use acetonitrile (ACN) or propylene carbonate (PC) as solvents, are commonly used for commercial supercapacitors. They are usually flammable and toxic. An alternative to organic-based electrolytes is aqueous electrolytes. One of the drawbacks of aqueous electrolytes is the limited cell voltage (~ 1 V) due to the narrow electrochemical stability window (~ 1.23 V). The development of alternative electrolytes focuses on increasing the cell voltage of SCs. The cell voltage of SCs in glycerol-based electrolytes supports a large potential window, which is twice greater than that of aqueous electrolytes. Glycerol, commonly called glycerin, is a by-product of FAME (fatty acid methyl ester) biodiesel. An estimated 1 kg of crude glycerol is produced per 10 kg of biodiesel produced. Glycerol-based electrolytes are non-toxic, relatively safe, low-cost, heat-resistant, and environmentally friendly.

Introduction

Due to the growing demand for energy consumption and the development of new energy sources, energy storage devices are needed for balancing the energy supply and demand on the electrical grid system. Among the different types of energy storage systems, electrochemical supercapacitors (SCs), also known as ultracapacitors, have drawn a lot of attention as they bridge the gap between electrolytic capacitors and batteries. SCs have high energy densities and can store more energy than electrostatic capacitors. In addition, SCs have high power densities and can store and release energy faster than batteries [1]. Other advantages of SCs include a long-life cycle (> 100,000 cycles), fast charge–discharge rates (from seconds to minutes), low maintenance, lightweight, and safe operations [2]. Due to its high self-discharge rate, SCs are not fitting for long-term energy storage [3]. In comparison to batteries, SCs have lower-energy storage capacity and are not well-suited for applications requiring high energy density [4]. Therefore, SCs can be used as a complement to other energy storage devices, such as batteries for electric vehicles, or for those applications requiring a lot of power in short bursts [5].

Based on the charge storage mechanism (faradaic and non-faradaic), supercapacitors are classified into three categories, namely electric double-layer capacitors (EDLCs), pseudocapacitors, and hybrid supercapacitors [6]. EDLCs store charge through physical adsorption–desorption of charged electrolyte ions at the surface of porous carbon-based electrodes; an electrostatic and non-faradaic mechanism [7]. Pseudocapacitors store charge through fast and reversible reduction–oxidation (redox) reactions at the surface or near-surface of the electrode. Thus, there is a transfer of charges at the electrode–electrolyte interfaces due to a faradaic mechanism [8]. Hybrid supercapacitors are based on two different mechanisms of charge storage: faradaic e non-faradaic. The negative electrode material, commonly a carbon-based electrode, is responsible for the power source and it stores charge non-faradaically. Otherwise, the positive electrode material, commonly a metal oxide electrode, is responsible for the energy source and it stores charge faradaically [1].

Electrodes and electrolytes are at the core of SCs research. Most research topics focus on electrode materials and only a few types of research focus on the study of electrolytes [9].

The electrochemical performance of electrodes depends on variables such as specific surface area (SSA), surface functional groups, and pore distribution. Due to high SSA, within a range of 500–2500 $m^2\ g^{-1}$, activated carbons (ACs) are common examples of carbon-based electrodes for EDLCs [10]. Examples of ACs include granular activated carbon (GAC) and powder activated carbon (PAC). In AC-based electrodes, binders are utilized to provide strong adhesion between the electrode and the current collector. These binders cause pore blockage reducing the active surface area of the electrode and increasing resistance which impacts the electrochemical performance of the supercapacitor [11]. Among the different types of activated materials, activated carbon fibers (ACF) can be converted into woven fabrics (yarn interlacing process), knit fabrics (yarn interlooping process), or felt (matted non-woven fabric) offering them self-supporting characteristics [12]. ACF-based electrodes, which are binder-free electrodes, have drawn attention not only because of high SSA (mostly micropores), but also due to a well-defined porous structure, and high adsorption capacity [13]. An example of a synthetic precursor used to produce ACFs is Polyacrylonitrile (PAN); a thermoplastic polymer with a high melting point of 350 °C [14]. Textile PAN-based fibers are low-cost and alternative raw materials used to produce ACFs [15]. In order to obtain self-supporting characteristics, textile PAN-based fibers are converted into a felt.

The application of textile PAN-based fibers as electrodes for supercapacitors in aqueous electrolytes, using a two-electrode setup, was reported in previous studies [15, 16]. In the former, a volumetric capacitance of 104 F cm^{-3} in H_2SO_4 2 mol L^{-1} was found. In the latter, electrodes decorated with silver particles exited a gravimetric capacitance of 169 F g^{-1} in KOH 6 mol L^{-1}. Another studied [17] about

textile PAN-based fiber electrodes, with enhanced surface functional groups, reported a gravimetric capacitance of 230 F g^{-1} in H_2SO_4 2 mol L^{-1} (three-electrode setup). A high gravimetric capacitance of 302 F g^{-1} in H_2SO_4 2 mol L^{-1} in a two-electrode setup was reported in a previous studied [18] about a binary composite based on polypyrrole and textile PAN-based fiber electrodes. In all previous studies, only aqueous electrolytes were investigated.

Carbon-based electrodes in organic electrolytes, which use acetonitrile (ACN) or propylene carbonate (PC) as solvents, are commonly used for commercial supercapacitors [4]. Although organic-based electrolytes can support a large potential window (~3 V), they are usually flammable and toxic [19]. Aqueous electrolytes are an alternative to organic-based electrolytes due to their advantages of high ionic conductivity (10^1–10^2 mS cm^{-1}), non-flammability, low cost, low internal resistance, and low viscosity [20]. One of the drawbacks of aqueous electrolytes is the limited cell voltage (~1 V) due to the narrow electrochemical stability window (~1.23 V). The development of alternative electrolytes focuses on increasing the potential window, also known as operating voltage, and consequently the energy density of the devices [21].

Glycerol (1,2,3-propanetriol), commonly called glycerin, is a by-product of FAME (fatty acid methyl ester) biodiesel. Accounting for 60% of the global glycerol market, FAME biodiesel is the major source of glycerol. It is estimated that 1 kg of crude glycerol is produced per 10 kg of biodiesel produced. Moreover, at a CAGR (compound annual growth rate) of 6.1%, the global glycerol market is expected to reach €2.92 billion by 2026. [22]. Glycerol ($C_3H_8O_3$) is an odorless, colorless, nontoxic, and nonirritating viscous liquid (1.5 Pa.s) with a high boiling point of 290 °C, a low melting point of 18 °C, and a density of 1.261 g cm^{-3} at 20° C. Glycerol monomer has a hydroxyl-rich structure with three hydroxyl functional groups (alcohol group), also known as trihydric alcohol. Due to its hydroxyl-rich structure, glycerol is highly hygroscopic and miscible in water [23]. In previous studies [24, 25] glycerol has been reported as a green solvent for organic synthesis. An early study on EDLCs [10] reported the use of glycerol as a plasticizer in solid polymer electrolytes. The addition of glycerol increased salt dissociation and decreased the bulk resistance of the electrolyte. Glycerol has also been reported in studies about deep eutectic solvents (DES) [26–28], a class of green electrolytes. DESs are composed of a hydrogen bond acceptor (HBA) such as a salt, and a suitable hydrogen bond donor (HBD). Potassium carbonate (K_2CO_3) [26], a basic salt, and choline chloride ($C_5H_{14}ClNO$) [27, 28], a quaternary ammonium salt, are examples of HBA, whereas glycerol is an example of HBD. Due to its high viscosity and hygroscopic properties, the use of glycerol as an alternative electrolyte for supercapacitors is still very limited, and there have not been many studies in this regard. Thus, the electrolyte used in this work has been based on a previous study carried out in bio-inspired redox mediated electrolyte for high-performance flexible supercapacitor applications over a broad temperature domain [29].

This work addresses EDLC storage devices and it has been divided into two parts, namely: (1) synthesis and characterization of binder-free electrodes from textile PAN-based fiber, and (2) electrochemical characterization of the electrodes in aqueous and glycerol-based electrolytes.

Experimental

Synthesis of Activated Carbon Fiber-Felt Electrodes From Textile PAN-Based Fiber

The synthesis of activated carbon fiber-felt (ACFF) electrodes was based on the methodology proposed in previous works [15, 17, 30] and included three fundamental processes: oxidation, carbonization, and physical activation (Fig. 1).

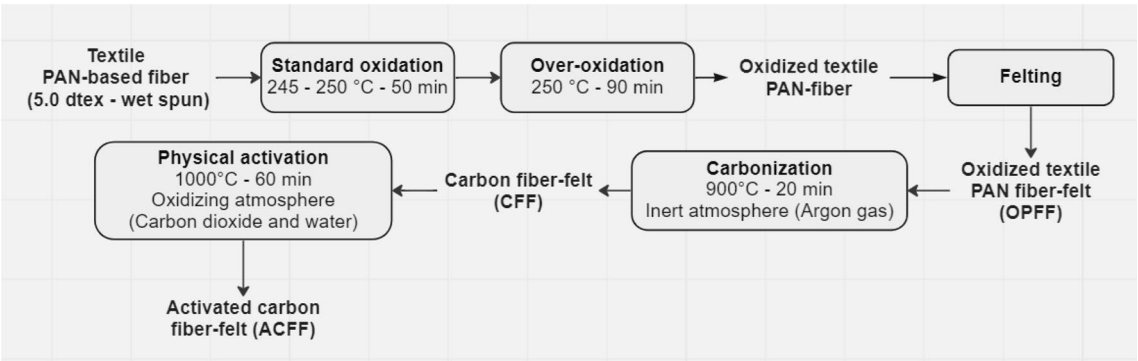

Fig. 1 Synthesis of ACFF electrodes

A wet-spun tow of textile PAN-based fiber (5.0 dtex), with a bean-type cross-section, was supplied by JMHP and used as a raw material to produce the felt. The fiber was transformed into a thermoset material through a two-step oxidation process, namely standard oxidation, and over-oxidation. Standard oxidation was performed in two steps over 50 min: a pre-oxidation at 245 °C and subsequent oxidation at 250 °C. According to the proposed methodology [17], oxidation time affects the surface chemistry of carbon-based materials and leads to the development of nitrogen groups. These nitrogen compounds, particularly the pyrrolic and the pyridinic functional groups, contribute to increased capacitance. Over-oxidation was carried out for 90 min at 250° C: totaling 140 min for the entire oxidation process.

Oxidized textile PAN fiber was converted into a felt (200 g m^{-2}) through a standard needle felting process (non-woven) and designated as oxidized textile-Pan fiber-felt (OPFF). The carbonization and physical activation of OPFF were carried out in a horizontal tube furnace. The OPFF sample, with a size of 0.30 m^2, a weight of 50 g, and 3 mm in thickness, was cut and placed in an appropriate sample holder. The carbonization of the OPFF sample was carried out under an inert atmosphere. The sample was heated from room temperature to 900 °C at a heating rate of 30 °C min^{-1} and 20 min of residence time. Subsequent carbonization and prior physical activation, the argon gas flow was switched off and replaced with carbon dioxide (200 sccm). A syringe was used to introduce a total of 12 ml of water during steam activation. Physical activation was carried out under an oxidizing atmosphere at 1000 °C and 60 min of residence time.

Subsequent physical activation, the gas flow was switched off and replaced with argon, and the furnace was turned off. The inert atmosphere was kept through the cooling process until room temperature. The activated carbon fiber-felt sample was designated as ACFF.

Textural and Structural Characterization of ACFF Electrodes

Textural and structural characterizations of the electrodes were carried out prior to the electrochemical characterizations. The surface textural properties of the ACFF samples were analyzed by Nitrogen (N_2) adsorption–desorption isotherms at 77 K using an ASAP 2020 Plus adsorption analyzer by Micromeritics. Specific surface area, average pore size, pore volume, pore size distribution and micropore volume were analyzed. Prior to the measurements, degasification of the sample was performed at 120 °C for 12 h under vacuum pressure of 5 µmHg. The structural characterization of ACFF samples was carried out by Raman-scattering spectroscopy technique using Horiba Scientific model Labram HR Evolution. Ar ion laser operating at 512 nm and scan mode of 1000—2500 cm^{-1} were employed to collect Raman spectra.

Electrolyte Selection

In order to understand the electrochemical behavior of the ACFF electrodes in aqueous and glycerol-based electrolytes, the following electrolytes were selected:

(1) Potassium hydroxide (KOH) solutions with molar concentrations of 1 mol L^{-1} and 2 mol L^{-1} were used as examples of conventional and strong alkaline electrolytes.
(2) Aiming to investigate green electrolytes, potassium hydroxide-glycerol hybrid electrolytes (KOH:GLYs) prepared with variations of viscosity and molar ratios of 1:1, 2:1, and 3:1 were used as glycerol-based electrolytes.

Assembly of the EDLC Cell

The ACFF sample was cut into small disks with a diameter of 8 mm and footprint area of 0.5 cm^2. In order to remove moisture, the ACFF electrodes underwent a drying process for 2 h at 110 °C. Subsequent drying, the electrodes were weighted and stored in a round vacuum desiccator. Before assembling the symmetric EDLC cell, moisture-free ACFF electrodes were immersed in aqueous electrolyte for 24 h (Fig. 2a). Due to the high viscosity of glycerol-based electrolytes and to improve electrolyte diffusion, electrode–electrolyte contact for approximately 2–3 h, at room temperature, is

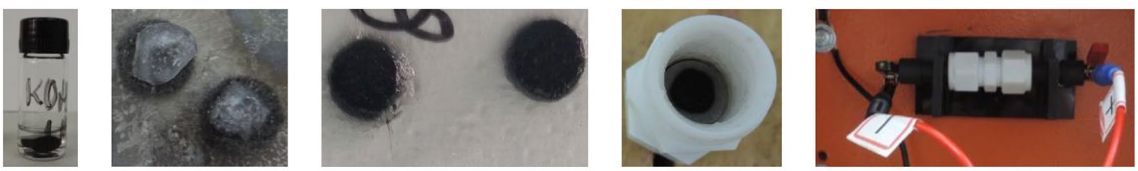

Fig. 2 **a** ACFF electrode immersed in aqueous electrolyte, **b** ACFF electrode impregnated with glycerol-based electrolyte before the diffusion process, **c** after the diffusion process **d** interior view of Swagelok®-cell, and **e** assembled symmetric EDLC

recommended (Fig. 2b). After electrolyte diffusion, ACFF electrodes impregnated with glycerol-based electrolytes were stored in vacuum desiccators for 48 h to remove moisture (Fig. 2c). A qualitative filter paper (0.2 mm in thickness) was cut into small disks with a diameter of 10 mm and used as a separator to keep the two electrodes apart and prevent a short circuit (Fig. 2d). Due to the self-supporting characteristics of the electrodes, binders are not required. Symmetric EDLC was assembled in a two-electrode Swagelok®-cell with a Teflon case and two graphite rods as current collectors (Fig. 2e). A Faraday cage was used to avoid external interferences. The active mass of the two parallel electrodes and the active mass loading are 6.5 ± 0.6 mg and 13.0 ± 1.3 mg cm^{-2}, respectively.

Electrochemical Characterization

Electrochemical impedance spectroscopy (EIS), cyclic voltammetry (CV), and galvanostatic charge–discharge (GCD) techniques were conducted to evaluate the performance and the electrochemical characteristics of ACFF electrodes in aqueous and glycerol-based electrolytes. Electrochemical measurements were carried out in a symmetric two-electrode configuration cell (Swagelok®-type) at room temperature in a multichannel potentiostat Parstat MC by Princeton Applied Research. Origin software version 9.70 was used for data analysis and graphing. Good practice for electrochemical characterization of supercapacitors, as those reported in previous works [31, 32], and an error of 10% in the values were taken into consideration.

CV was used to determine the total capacitance and the gravimetric capacitance of the EDLC devices. Capacitance (C), which is the ability to store charge per volt, is given in units of Farads (F), and it was calculated from the integration of the area under the CV curve according to Eq. 1 [33]:

$$C_{T(CV)}\left(\frac{\int_{V_1}^{V_2} i(V)d(V)}{2v(V_2 - V_1)}\right) \tag{1}$$

where C_T is the total capacitance of the cell (F), $\int_{V_1}^{V_2} i(V)d(V)$ is the area under the curve (V A), v is the scan rate (V s^{-1}), and $V_2 - V_1$ is the potential difference (V). The gravimetric capacitance of the cell (C_s) was calculated according to Eq. 2 [34]:

$$C_{s(CV)} = \frac{4C_T}{m} \tag{2}$$

where C_s is given in units of Farads per gram (F g^{-1}), and m is the total active mass of the electrodes (g).

CV measurements were conducted at a scan rate of 1 mV s^{-1} for both aqueous and glycerol-based electrolytes. Due to water electrolysis (decomposition at 1.23 V) [35], CV measurements of aqueous electrolytes were carried out within a potential window of 0—1 V. Taking into consideration the wide electrochemical stability window of glycerol-based electrolytes, measurements were carried out within a potential window of 0 – 2.1 V.

GCD and EIS experiments for aqueous and glycerol-based electrolytes were carried out at the same condition. EIS, a frequency response technique, was applied to analyze the interaction at the electrode–electrolyte interface. EIS measurements were performed with a frequency range of 10^{-3} Hz–10^{6} Hz, applied signal amplitude of 5 mV, applied potential of 0 V, and it was expressed graphically in a Nyquist plot.

GCD was used to determine the equivalent series resistance (ESR), also known as internal resistance, of the EDLC devices. As the voltage drop (IR_{drop}) is related to the internal resistance of the cell when the current is interrupted or inversed, the value of ESR was deduced according to Eq. 3 [36]:

$$ESR = \left|\frac{IR_{drop}}{2I}\right| \tag{3}$$

where ESR is given in units of Ohms (Ω), I is the applied current (A), and IR_{drop} is the voltage drop (V). GCD measurements were conducted at a potential window of 0—1 V at various current densities.

The total capacitance of the cell (Eq. 4), obtained in the GCD test, was used to determine the specific energy density (Eq. 5), which is the amount of energy stored per unit of weight [36].

$$C_{T(GCD)} = \frac{(I_{(discharge)} - (t_i - t_f))}{(V - IR_{drop})} \tag{4}$$

where $C_{T(GCD)}$ is given in units of Farads (F), $I_{(discharge)}$ is the discharge current (A), $(t_i - t_f)$ is the time difference (s), and (V) is the maximum potential (V).

$$E_D = \frac{1}{2}\frac{C_{T(GCD)}V^2}{3600m} \tag{5}$$

where E_D is given in units of watt-hours per kilogram (Wh kg^{-1}), m is the total active mass of the electrodes (kg), and 3600 (s) was used to convert Joule (J) to watt-hour (Wh).

Specific power density (P_D), which is the maximum power output per unit of mass, depends on the voltage and on the internal resistance of the cell (ESR). P_D was calculated according to Eq. 6 [37]:

$$P_D = \frac{V^2}{4ESRm} \tag{6}$$

where P_D is given in units of watt per kilogram (W kg^{-1}), and *ESR* is the internal resistance of the cell (Ω).

The Coulombic efficiency of the cell (η), which is the ratio of the discharging time and the charging time, was calculated using Eq. 7 [38]:

$$\eta = \frac{T_d}{T_c}100 \tag{7}$$

where (η) is expressed as a percentage by multiplying the ratio by 100, (T_c) is the charging time (s), and (T_D) is the discharging time (s).

Results and Discussion

Synthesis of ACFF Electrodes From Textile PAN-Based Fiber

The purpose of oxidation is to provide a structure that can withstand high temperatures and to prevent degradation and melting of the fiber in the subsequent carbonization process. Thermoplastic textile PAN-based fibers are converted into thermosetting fibers due to the cyclization of nitrile groups and the cross-linking of PAN chains [39]. Once stabilized, the PAN-based sample containing carbon and noncarbon elements, such as nitrogen, hydrogen, and oxygen, undergoes a carbonization process. As a result, noncarbon elements are removed and released as volatile gases resulting in weight loss and shrinkage of the sample [40].

Activation is the key process in the synthesis of carbon-based electrodes. During the activation process, existing clogged pores that were developed during carbonization are opened up and enlarged. In addition, new porosity is developed resulting in a well-defined porous structure and an enhanced surface area [19]. Physical activation requires high temperatures (700–1200 °C) and some of the carbon atoms are removed during the process resulting in low production yield [41, 42]. CO_2 leads to a higher development of narrow microporosity, and hence it was chosen as the major oxidizing agent. As a combination of two oxidizing agents contributes to the development of enhanced porosity, water (steam) was chosen as the minor oxidizing agent. While CO_2 leads to the development of new microporosity, water helps to widen the existing micropores. Since water requires lower temperatures in comparison to CO_2, water was used in the first stage of the activation process. If the activation time is overextended, the development of mesopores (between 2 and 50 nm) occurs by burning off the wall bordering the micropores (> 2 nm) [43]. After the carbonization-activation process, the ACFF sample had a production yield of 21%, a total mass loss of 79%, and a shrank of 43% in size.

Characterization of the ACFF Electrodes

According to the IUPAC classification of adsorption Isotherms for gas–solid equilibria [44], the N_2 adsorption–desorption isotherm of ACFF electrodes, shown in Fig. 3a, is classified as Type I and indicates a microporous character. Moreover, hysteresis is absent, which suggests that the size of the pores measured on both adsorption and desorption branches coincides well. [45, 46]. BET theory was applied to calculate the specific surface area (S_{BET}) of ACFF electrodes from the acquired data of N_2 adsorption at 77 K. In accordance with the results, ACFF electrodes have a high S_{BET} value of 1875 m^2 g^{-1} and a correlation coefficient (r) of 0.999918. Compared with previous works [15, 30], the S_{BET} of ACFF electrodes produced in this work is about

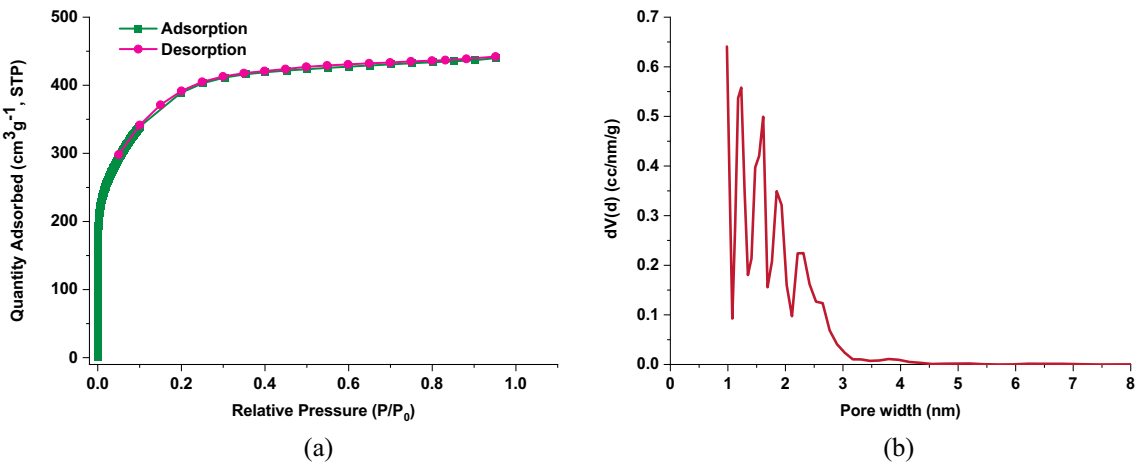

Fig. 3 ACFF electrodes **a** nitrogen adsorption–desorption isotherm and **b** pore size distribution

1.5 times higher. The microporosity developed particularly during the activation process contributed to the high value of the specific surface area.

The mobility of the ions into the pores depends on the pore size. Thus, inaccessible pores do not contribute to both double-layer capacitance and energy density [47]. Previous studies suggested that pore size smaller than 0.5 nm is inaccessible to hydrated ions [48, 49]. The technique applied for pore size distribution (Fig. 3b) does not show any information about pores smaller than 1 nm due to the penetration limit of N_2. Regardless of the limitation, an ascending line in the region of pore width smaller than 1 nm possibly indicates the presence of said micropores [15]. The pore size distribution curve determined by the DFT method shows a maximum pore width of 3 nm. As reported in the literature, a small number of pores, wider than 2 nm, increase the power density of SCs [50]. These small mesopores facilitate the access of electrolyte ions into the electrode surface. Furthermore, most pores vary in size from 1 to 2 nm with a modal distribution of 1.2 nm. The average pore size of PAN-based ACF reported in the literature ranges from 4 to 10 nm [51]. The average pore size of the ACFF sample is smaller due to the parameters of the activation process. The development of porosity is influenced by several factors such as the residence time, temperature, original porosity and structure of the carbonized material, pressure and flow rate of the gas, and the type of oxidizing agent [52]. Additionally, the volume of micropores (0.69 $cm^3\ g^{-1}$) in the ACFF electrodes is equivalent to 87% of the total volume of pores (0.79 $cm^3\ g^{-1}$) confirming high microporosity. In comparison to previous works [15, 30], the volume of micropores and the total volume of pores are about 1.3 times higher.

The Raman spectrum for carbon-based materials, amorphous or crystalline, exhibits two well-defined peaks commonly assigned as D and G bands. The D band, also known as the disorder/defect band, exhibits a peak at nearly 1380 cm^{-1}. The G band, crystalline graphite, exhibits a peak at nearly 1580 cm^{-1} due to the C–C bond-stretching of all pairs of sp^2 atoms in both rings and chains [53]. The Raman spectra of the ACFF electrode, in five different regions of the same sample, are shown in Fig. 4. In all regions, the spectra exhibited the same appearance. There are two very broad peaks located in the range of 1244 – 1710 cm^{-1}. The first peak, located at 1342 cm^{-1}, is referred to "D". The second peak, located at 1598 cm^{-1} is referred to "G". The spectra of ACFF electrodes are very similar to that of carbon-based materials presented in previous works [17, 18].

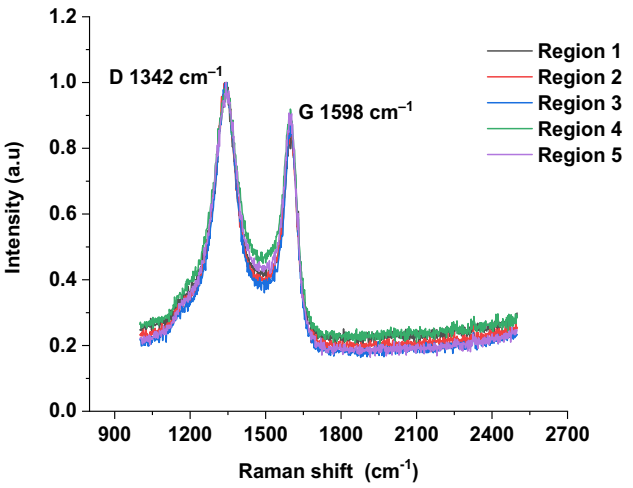

Fig. 4 Raman spectra obtained in five different regions of the same sample

Electrochemical Performance

The CV curves of ACFF-based EDLCs in aqueous and glycerol-based electrolytes, at a scan rate of 1 m V s^{-1}, can be seen in Fig. 5. As capacitance is constant over an acknowledged potential window, rectangular curves are expected in the cyclic voltammogram for an ideal capacitive behavior [54]. Nevertheless, actual EDLCs exhibit nearly rectangular CV curves with blunt corners due to the equivalent series resistance of the cell (ESR) [55]. Therefore, in comparison to glycerol-based electrolytes, aqueous electrolytes (Fig. 5a) exhibited less distorted rectangular-shaped curves that indicate low values for ESR and a charge storage mechanism that is mostly electrostatic (non-faradaic). Moreover, the tail observed in the CV curves of aqueous electrolytes suggests electrochemical decomposition of the electrolyte, at high potentials, due to water electrolysis [56]. The narrow potential window (≈ 1 V) of aqueous electrolytes is a drawback since it limits energy density and restricts the amount of energy stored [57].

KOH:GLY at a molar ratio of 1:1 (Fig. 5b), exhibited CV curves with rounded corners that deviated from the linearity and suggests high values for ESR. Furthermore, the tail observed in the CV curves of KOH:GLYs, particularly at molar ratios of 1:1 and 2:1, possibly indicates the presence of water content due to the fact that both components of the glycerol-based electrolyte are hygroscopic. Thereby, the highest gravimetric capacitance value of 99 ± 10 F g^{-1} obtained in KOH:GLY (2:1), possibly occurred due to the additional long tail, which could affect overall electrochemical performance and may not represent an actual value for the gravimetric capacitance. KOH:GLY (3:1), exhibited a specific capacitance value of 82 ± 8 F g^{-1}, less distorted rectangular-shaped curves and a much shorter tail, which suggests a better capacitive behavior and lower resistance (Fig. 5b). Among the ACFF-based EDLCs, aqueous KOH electrolyte at a molar concentration of 2 mol L^{-1} (Fig. 5a) exhibited the highest gravimetric capacitance value of 129 ± 13 F g^{-1}.

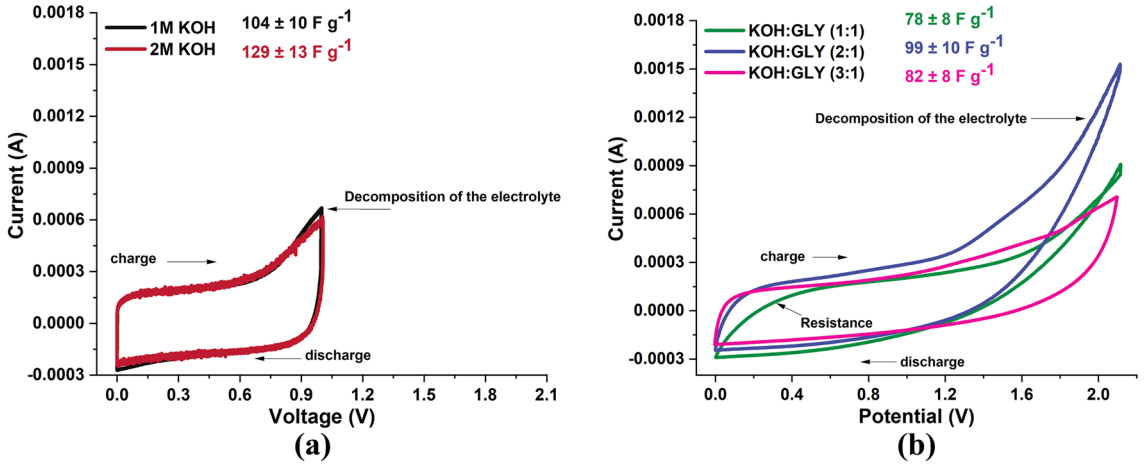

Fig. 5 CV curves of ACFF-based EDLCs at a scan rate of 1 mV s^{-1} **a** in aqueous electrolytes and **b** glycerol-based electrolytes

The absence of humps or peaks in the CV curves of ACFF-based EDLCs suggests that there is no occurrence of oxidation–reduction (redox) reactions, which is expected from an electrostatic and non-faradaic mechanism [58]. Nevertheless, previous literature reported that carbon-based electrodes possibly exhibit 1 – 5% of their capacitance as surface-redox pseudocapacitance due to reversible faradaic-redox reactions of active surface functional groups [59]. A previous work [17], synthesized a similar electrode material through a two-step oxidation process. The results of the XPS analysis showed that the oxygen and the nitrogen groups found in the textile PAN-based electrode are 3.86% and 1.36% in mass, respectively. As explained previously, oxidation time affects the surface chemistry of AC-based materials leading to enhanced capacitance. In this work, the occurrence of a minor surface-redox pseudocapacitive behavior could be verified with a three-electrode cell, at a low scan rate, instead of a two-electrode cell.

Figure 6 shows the Nyquist plot for aqueous and glycerol-based electrolytes at an applied potential of 0 V; where $-Z_{im}$ is the imaginary part (capacitive) and Z_{re} is the real part (resistive) [60]. A Nyquist plot exhibits three distinct frequency regions: (1) a high-frequency region that is higher than 10 kHz (low values for Z_{re}), (2) a medium-frequency region, ranging from 10 kHz to 1 Hz, and (3) a low-frequency region that is lower than 1 Hz (high values for Z_{re}) [61].

At high frequencies, supercapacitors exhibit a resistive behavior that is related to the bulk solution resistance of the electrolyte [62]. The value of electrolyte resistance (R_s) can

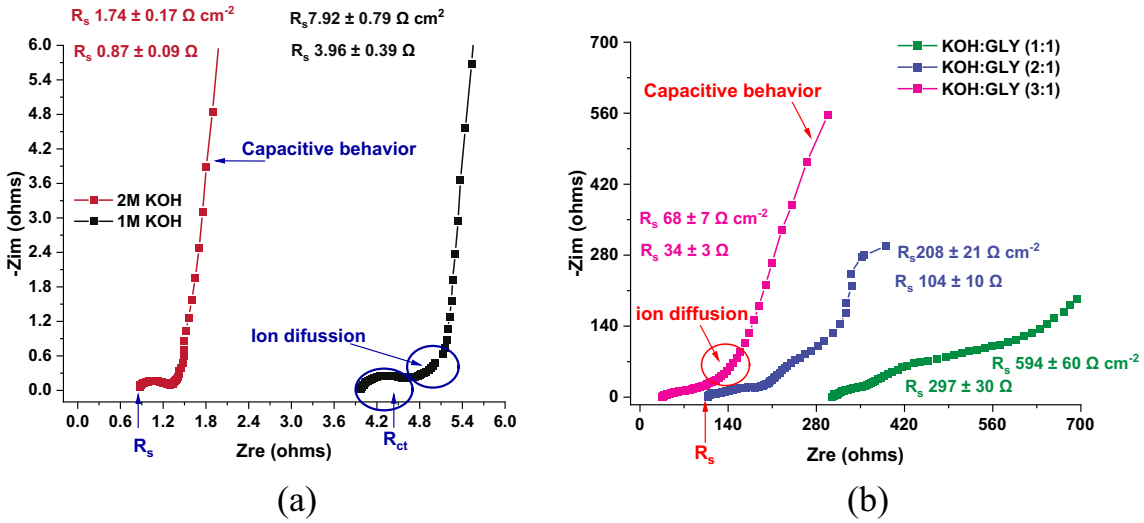

Fig. 6 Nyquist plots of ACFF-based EDLCs **a** in aqueous electrolytes and **b** in glycerol-based electrolytes

be deduced at the point where the plot intercepts the x-axis (Z_{re}) of the Nyquist plot [63]. The results are normalized by Ω cm^{-2} for comparison. Aqueous electrolytes have low electrolyte resistance in comparison to glycerol-based electrolytes. Among aqueous electrolyte, KOH electrolyte, at a molar concentration of 2 mol L^{-1} (Fig. 6a), has the lowest R_s of 0.87 ± 0.09 Ω (1.74 ± 0.17 Ω cm^{-2}). Among glycerol-based electrolytes (Fig. 6b), the lowest R_s of 34 ± 3 Ω (68 ± 7 Ω cm^{-2}) was found in KOH:GLY (3:1) probably due to the salt concentration as conductivity can be affected by the salt-to-solvent ratio [64].

The interfacial impedance between the bulk solution (electrolyte) and the electrode can be observed at medium frequencies. A conventional Nyquist plot for an EDLC cell exhibits a single semicircle that represents the ion charge-transfer resistance (R_{ct}) [55]. A single semicircle can be seen in both concentrations of aqueous electrolytes. The values of R_{ct} for 1 M KOH and 2 M KOH are 0.59 ± 0.06 Ω (1.18 ± 0.12 Ω cm^{-2}) and 0.36 ± 0.04 Ω (0.72 ± 0.07 Ω cm^{-2}), respectively. After the semicircle, a 45-degree line, or slope, at the low frequency region indicates ion diffusion within the pores [65]. While 2 M KOH exhibits a steep slope after the semicircle, 1 M KOH and KOH:GLY (3:1) exhibit gradual slopes. A steep slope suggests that ion penetration into pores occurs efficiently. A gradual slope, as in the case of 1 M KOH and KOH:GLY (3:1), suggests that ion penetration into pores occurs laboriously [16].

A vertical line at the low-frequency region parallel to the imaginary part (y-axis) is expected for an ideal capacitor [44]. The 90-degree line, or tail, suggests that capacitance is constant over the applied frequency range and the electrode surface is entirely impregnated [65]. A vertical line can be observed in the Nyquist plot for both concentrations of aqueous electrolytes (Fig. 6a), and a nearly vertical line can be observed in the glycerol-based electrolyte KOH:GLY (3:1) (Fig. 6b). The Nyquist plots of KOH:GLY with molar ratios of 1:1 and 2:1 deviate from the profile expected from an ideal EDLC.

In comparison to aqueous electrolytes, glycerol-based electrolytes have high electrolyte resistance. Due to the low viscosity of its solvent, aqueous electrolytes have high ionic conductivity which improves ion mobility and results in smaller values for R_s and R_{ct} [20, 54]. On the contrary, glycerol-based electrolytes (Fig. 2b) have high viscosity and do not provide good contact in the electrode–electrolyte interface. As ion mobility is inversely proportional to the size of the ion, large molecules, such as glycerol molecules, have high resistivity. Thus, large pores in the surface of the electrode are required since inaccessible pores do not contribute to the double layer capacitance [54].

The GCD curves of ACFF-based EDLCs in glycerol-based and aqueous electrolytes can be seen in Figs. 7 and 8, respectively. Isosceles or quasi-isosceles triangular-shaped curves, which predominantly suggest an electrostatic mechanism (non-faradaic), are expected for carbon-based EDLC devices [66]. Among the ACFF-based EDLCs, the discharge curve of both aqueous electrolytes and KOH:GLY (3:1) drop linearly indicating that there is no considerable contribution of pseudocapacitance since the charge storage mechanism is mainly electrostatically [65].

At a current density of 0.15 ± 0.02 A g^{-1} (Fig. 7a), the charge curve of KOH:GLY (3:1) is asymmetrical to its corresponding discharge curve due to a noticeable IR_{drop} (resistance), resulting in quasi-isosceles triangular-shaped curves, a Coulombic efficiency of 90%, a gravimetric capacitance of 64 ± 6 F g^{-1}, and an internal resistance (ESR) of 64 ± 6 Ω (128 ± 13 Ω cm^{-2}). Among glycerol-based electrolytes, KOH:GLY (3:1) exhibited the lowest ESR value and a better electhochemical performance as electrolyte conductivity can be affected by the salt-to-solvent ratio. Due to the non-linearity of the GCD curves and a resistive rather than capacitive behavior, the GCD curves of KOH:GLYs (2:1)

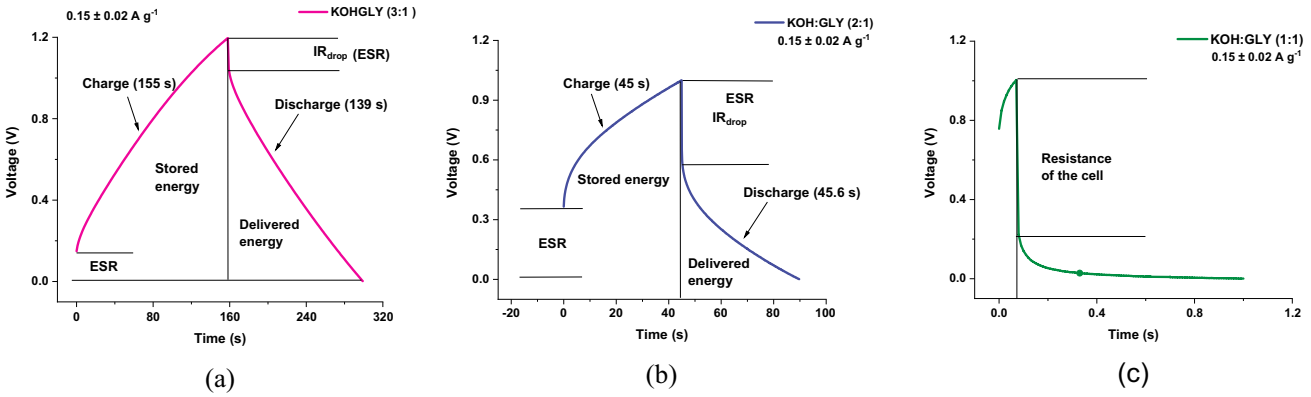

Fig. 7 GCD curves of ACFF-based EDLCs in glycerol-based electrolytes at a current density of 0.15 ± 0.02 A g^{-1} **a** KOH:GLY (3:1), **b** KOH:GLY (2:1), and **c** KOH:GLY (1:1)

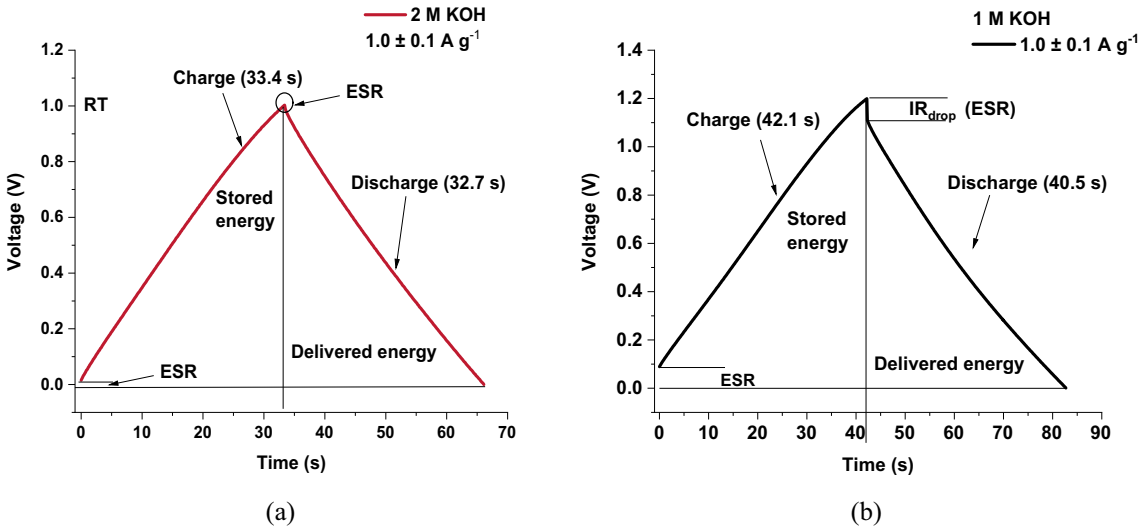

Fig. 8 GCD curves of ACFF-based EDLCs in aqueous electrolytes at a current density of 1.0 ± 0.1 A g^{-1} **a** in 2 M KOH and **b** in 1 M KOH

and (1:1) deviate from the profile expected from an ideal EDLC (Fig. 7b and c, respectively). At a current density of 0.15 ± 0.02 A g^{-1}, the GCD curves of KOH:GLY (2:1) are overcharged, thus resulting in a Coulombic efficiency of 101%. At this molar ratio, the gravimetric capacitance and the internal resistance of the cell are 42 ± 4 F g^{-1} and 188 ± 19 Ω (376 ± 38 Ω cm^{-2}), respectively.

The occurrence of IR-drop in aqueous electrolytes is not noticeable in small current densities, such as the current density of 0.15 A g^{-1} applied in glycerol-based electrolytes. Due to the nature of aqueous electrolytes, such as high conductivity and low viscosity, larger current densities are required. At a current density of 1.0 ± 0.1 A g^{-1}, the curve of 2 M KOH (Fig. 8a) is charged and discharged within almost the same time frame, resulting in isosceles triangular-shaped curves, a Coulombic efficiency of 98%, a gravimetric capacitance of 103 ± 10 F g^{-1}, and an internal resistance of 1.74 ± 0.17 Ω (3.48 ± 0.35 Ω cm^{-2}). In contrast, the charge curve of 1 M KOH (Fig. 8b) is asymmetrical to its corresponding discharge curve due to a noticeable ESR, resulting in quasi-isosceles triangular-shaped curves, a Coulombic efficiency of 96%, a gravimetric capacitance of 86 ± 9 F g^{-1}, and an internal resistance (ESR) of 9.03 ± 0.9 Ω (18.1 ± 1.8 Ω cm^{-2}).

Specific energy density (E_D) and specific power density (P_D) were determined at different current densities from the total capacitance and the internal resistance of the cell, respectively. It should be noted that KOH:GLYs (2:1) and (1:1) did not support the current density applied, thus E_D and P_D were not determined.

Previous literature reported that the specific energy and the specific power of EDLCs commonly range from 1 to 6 Wh kg^{-1} and 2 to 20 kW kg^{-1}, respectively [36]. As can be seen in Table 1, due to a better capacitive behavior, 2 M KOH exhibited the highest E_D of 3.3 ± 0.3 kW kg^{-1}. The E_D of KOH:GLY (3:1) is 2.2 ± 0.2 kW kg^{-1}. Although E_D of KOH:GLY (3:1) has a lower value than that of aqueous electrolytes, it remains promising. Energy density is proportional to the capacitance and the square voltage of the cell. As a result, increasing either or both enhances the energy density of EDLCs and expands the range of SCs applications.

Table 1 Specific energy density (E_D) and specific power density (P_D) of aqueous and glycerol-based electrolytes

Type of electrolyte		E_D (Wh kg^{-1})	P_D (kW kg^{-1})
Aqueous	1 M KOH	2.8 ± 0.3	4.0 ± 0.4
	2 M KOH	3.3 ± 0.3	27.9 ± 2.8
Glycerol-based	KOH:GLY (3:1)	2.2 ± 0.2	0.6 ± 0.1

ESR limits power density and the energy cannot be delivered completely due to the distance between the electrolyte and the electrode, and the contact resistance between the current collector and the electrode [10]. Due to low internal resistance, 2 M KOH exhibited the highest P_D of 27.9 ± 2.8 kW kg^{-1}, which is 7 and 46 times greater than that of 1 M KOH and KOH:GLY (3:1), respectively. In order to improve the specific power of glycerol-based electrolytes, decreasing the value of ESR and improving ionic conductivity and mobility is suggested.

The results are in agreement with the Nyquist plot and the cyclic voltammogram data discussed in the preceding section. Aqueous electrolytes have high ionic conductivity and wettability which enhance electrode–electrolyte interaction and consequently decrease ESR values offering a better electrochemical performance.

Although the presence of a metallic catalyst is necessary for the electro-oxidation of glycerol to occur, there is a possibility that for a certain potential the electro-oxidation of glycerol might occur on the activated carbon fiber-felt electrode. In fact, the oxidation of glycerol over glassy carbon-supported Au nanoparticles in alkaline medium has already been investigated by cyclic voltammetry [67]. It has been verified that there is an effect of the carbon support on the activity of the glassy carbon-supported Au nanoparticles. The results from this study about the oxidation of glycerol and ethylene glycol on Au and Pt nanoparticles supported on the glassy carbon indicated that the carbon support participates actively in the oxidation of glycerol and other alcohols. It has been proposed that active oxygenated species were gradually formed on the glassy carbon surface by potential cycling, and these oxygenated species on carbon were additional oxygen suppliers to the oxidation of glycerol residues adsorbed on the Au particles [67]. In the present investigation, the possibility of electro-oxidation of the glycerol on a carbon-based electrode was assumed non-occurring due to the high purity of the activated carbon fiber-felt electrode (C = 94.5%, O = 3.86%, and N = 1.36% [17]).

Conclusions

The synthesis of activated carbon fiber-felt electrodes (ACFF) via two-step oxidation, carbonization, and physical activation resulted in low-cost and binder-free electrodes with a specific surface area of 1875 $m^2\ g^{-1}$ containing 87% of the total volume of pores as micropores, maximum pore width of 3 nm, and the size of most pores ranging from 1 to 2 nm. ACFF electrodes are suitable for aqueous electrolytes, particularly 2 M KOH. ACFF-based EDLC in 2 M KOH exhibited a gravimetric capacitance value of 129 ± 13 $F\ g^{-1}$ at 1 mV s^{-1}, low internal resistance (1.74 ± 0.17 Ω at 1 A g^{-1}), and low electrolyte resistance (0.87 ± 0.09 Ω). Although aqueous electrolytes have high conductivity and low viscosity, the cell voltage is limited (~ 1 V) due to the narrow electrochemical stability window. KOH:GLY at molar ratio of 3:1, a glycerol-based electrolyte, supports a potential window that is twice greater than that of aqueous electrolytes. ACFF-based EDLC in KOH:GLY (3:1) exhibited an electrolyte resistance of 34 ± 3 Ω, an internal resistance of 64 ± 6 Ω (at 0.15 ± 0.02 A g^{-1}), and a gravimetric capacitance of 82 ± 8 $F\ g^{-1}$ (at 1 mV s^{-1}). Although high resistance and high viscosity are drawbacks in electrochemical performance, glycerol-based electrolyte (KOH:GLY 3:1) is a low-cost, non-toxic and heat-resistant hybrid green-electrolyte.

The electrochemical performance of supercapacitors strongly relies on the electrode–electrolyte interaction and correlating the size of electrolyte ions and the pore size of carbon-based electrodes is necessary. Glycerol-based electrolytes have large molecules that are not well-fitting for the pore width of the ACFF electrode synthesized in this work. Inaccessible pores do not contribute to double-layer capacitance, and it is suggested to change the parameters of the physical activation process. The viscosity of the electrolyte and consequently ion mobility and ion diffusion could be improved by heating. Although this field is still very limited and there have not been many studies on this subject, glycerol-based electrolytes are promising electrolytes for supercapacitors, especially given that glycerol is a by-product of FAME biodiesel.

Author Contributions All authors contributed to the study conception and design. Material preparation, data collection and analysis were performed by Ingrid Ariani Belineli Barbosa, Jossano Saldanha Marcuzzo, Ivana Conte Cosentino and Rubens Nunes de Faria Junior. The first draft of the manuscript was written by Ingrid Ariani Belineli Barbosa and all authors commented on previous versions of the manuscript. All authors read and approved the final manuscript.

Funding This work was supported by the Academic Excellence Program (PROEX) within the Coordination for the Improvement of Higher Education Personnel (CAPES). Textile Pan-based fiber was supplied by JMHP Carbon.

Data Availability The datasets generated during and/or analyzed during the current study are available from the corresponding author on reasonable request.

Declarations

Conflict of Interests The authors have no competing interests to declare that are relevant to the content of this article.

References

1. Yang, Y., Han, Y., Jiang, W., Zhang, Y., Xu, Y., Ahmed, A. M.: Application of the supercapacitor for energy storage in China: role and strategy. Appl Sci (2021). doi:https://doi.org/10.3390/app12010354.
2. Scibioh, M.A., Viswanathan, B.: Supercapacitor: an introduction. In: Materials for supercapacitor applications, pp. 1–13. Elsevier (2020).
3. Shang, W., Yu, W., Xiao, X., Ma, Y., He, Y., Zhao, Z., Tan, P.: Insight into the self-discharge suppression of electrochemical capacitors: Progress and challenges. Adv Powder Mater (2023). https://doi.org/10.1016/j.apmate.2022.100075
4. González, A., Goikolea, E., Barrena, J.A., Mysyk, R.: Review on supercapacitors: Technologies and materials. Renew. Sustain. Energy Rev. (2016). https://doi.org/10.1016/j.rser.2015.12.249
5. Kurzweil, P.: Typical applications – electrochemical double-layer capacitors. In: Electrochemical energy storage for renewable sources and grid balancing, pp. 352. Elsevier (2015).
6. Pore, O.C., Fulari, A.V., Shejwal, R.V., Fulari, V.J., Lohar, G.M.: Review on recent progress in hydrothermally synthesized MCo_2O^4/rGO composite for energy storage devices. Chem. Eng. J. (2021). https://doi.org/10.1016/j.cej.2021.131544

7. Sagadevan, S., Marlinda, A.R., Chowdhury, Z.Z., Wahab, Y.B.A., Hamizi, N.A., Shahid, M.M., Mohammad, F., Podder, J. Johan, M.R.: Fundamental electrochemical energy storage systems. In: Advances in supercapacitor and supercapattery, pp. 31–37. Elsevier (2021).
8. Yu, A., Chabot, V., Xhang, J.: Fundamentals of electrochemical pseudocapacitors. In: Electrochemical supercapacitors for energy storage and delivery, pp 99–102. CRC Press (2013).
9. Bhat, T.S., Patil, P.S., Rakhi, R.B.: Recent trends in electrolytes for supercapacitors. J Energy Storage (2022). https://doi.org/10.1016/j.est.2022.104222
10. Aziz, S.B., Hamsan, M.H., Brza, M.A., Kadir, M.F.Z., Muzakir, S.K., Abdulwahid, R.T.: Effect of glycerol on EDLC characteristics of chitosan:methylcellulose polymer blend electrolytes. J. Mater. Res. Technol. (2020). https://doi.org/10.1016/j.jmrt.2020.05.114
11. Mistry, A., Trask, S., Dunlop, A., Jeka, G., Polzin, B., Mukherjee, P.P., Srinivasan, V.: Quantifying negative effects of carbon-binder networks from electrochemical performance of porous li-ion electrodes. J. Electrochem. Soc. (2021). https://doi.org/10.1149/1945-7111/ac1033
12. Ahmed, F.M., Reda, M.M., El-Aziz, H.A.A., Othman, H.A.: Overview of different fabric structures. J. Text. Color. Polym. Sci. (2022). https://doi.org/10.21608/jtcps.2022.152641.1131
13. Chen, J.Y.: Activated carbon fiber – Introduction. In: Activated carbon fiber and textiles, pp. 4–5. Woodhead Publishing Series in Textiles (2017).
14. Yue, Z., Economy, J..: Thermooxidative stabilization of PAN fibers. In: Activated Carbon Fiber and Textiles, pp. 64–66. Woodhead Publishing Series in Textiles (2017).
15. Marcuzzo, J.S., Cuña, A., Tancredo, N., Mendez, E., Bernardi, H.H.: Microporous activated carbon fiber felt from Brazilian textile PAN fiber: preparation, characterization, and application as super capacitor electrode. Rev. Bras. Apl. Vac. (2016). https://doi.org/10.17563/rbav.v35i2.1022
16. Rodrigues, A.C., Silva, E.L., Quirino, S.F., Cuna, A., Marcuzzo, J.S., Matsushima, J.T., Gonçalves, E.S., Baldan, M.R.: Ag@ Activated carbon felt composite as electrode for supercapacitors and a study of three different aqueous electrolytes. Mater. Res. (2019). https://doi.org/10.1590/1980-5373-MR-2018-0530
17. Rodrigues, A.C., Munhoz, M.G.C., Pinheiro, B.S., Batista, A.F., Amaral-Labat, G.A., Cuña, A., Matsushima, J.T., Marcuzzo, J.S., Baldan, M.R.: N-activated carbon fiber produced by oxidation process design and its application as supercapacitor electrode. J. Porous Mater. (2020). https://doi.org/10.1007/s10934-019-00799-7
18. Matsushima, J.T., Rodrigues, A.C., Marcuzzo, J.S., Cuna, A., Baldan, M.R.: 3D-interconnected framework binary composite based on polypyrrole/textile polyacrylonitrile-derived activated carbon fiber felt as supercapacitor electrode. J. Mater. Sci.: Mater. Electron. (2020). https://doi.org/10.1007/s10854-020-03568-4
19. Taer, E., Febriyanti, F., Apriwandi, Taslim, R., Augustino, Mustika, W.S.: Investigation of H_2SO_4 and KOH aqueous electrolyte on the electrochemical performance of activated carbon derived from areca catechu husk. J Phys (2021). doi:https://doi.org/10.1088/1742-6596/1940/1/012033.
20. Chen, J., Lee, P.: Electrochemical supercapacitors: from mechanism understanding to multifunctional applications. Adv. Energy Mater. (2021). https://doi.org/10.1002/aenm.202003311
21. Scibioh, M.A., Viswanathan, B.: Introduction – electrolyte materials for supercapacitors. In: Materials for supercapacitor applications, pp. 207–208. Elsevier (2020).
22. PNO: Market Analysis and Stakeholders report. In: EU project GLAMOUR – Glycerol to Biofuel: market, technologies, and players. https://www.pnoconsultants.com/innovationservices/wp-content/uploads/sites/9/2022/12/Glamour-report-glycerol-to-biofuel.pdf (2020). Accessed 6 May 2023.
23. Pagliaro, M.: Properties, applications, history, and market. In: Glycerol, pp. 1–6. Elsevier (2017).
24. Díaz-Álvarez, A.E., Cadierno, V.: Glycerol: a promising green solvent and reducing agent for metal-catalyzed transfer hydrogenation reactions and nanoparticles formation. Appl. Sci. (2013). https://doi.org/10.3390/app3010055
25. Lenardão, E.J., Barcellos, A.M., Penteado, F., Alves, D., Perin, G.: Glycerol as a solvent in organic synthesis. Revista Virtual de Química (2017). https://doi.org/10.21577/1984-6835.20170015
26. Naser, J., Mjalli, B., Jibril, S., Al-Hatmi, Gano, Z.: Potassium carbonate as a salt for deep eutectic solvents. Int J Chem Eng Appl (2013). doi: https://doi.org/10.7763/IJCEA.2013.V4.275.
27. Cojocaru, A., Brincoveanu, O., Pantazi, A., Balan, D., Enaschescu, M., Visan, T., Anicai, L.: Electrochemical preparation of Ag nanoparticles involving choline chloride – glycerol deep eutectic solvents. Bulgarian Chem Commun Special Issue **49**, 194–204 (2017)
28. Faraone, A., Wagle, D.V., Baker, G.A., Novak, E.C., Ohl, M., Reuter, D., Lunkenheimer, P., Loidl, A., Mamontov, E.: Glycerol hydrogen-bonding network dominates structure and collective dynamics in a deep eutectic solvent. J. Phys. Chem. (2018). https://doi.org/10.1021/acs.jpcb.7b11224
29. Cevik, E., Gunday, S.T., Bozkurt, A., Amine, R., Amine, K.: Bio-inspired redox mediated electrolyte for high performance flexible supercapacitor applications over broad temperature domain. J. Power Sources (2020). https://doi.org/10.1016/j.jpowsour.2020.228544
30. Junior, M.A.A., Matsushima, J.T., Rezende, M.C., Gonçalves, E.S., Marcuzzo, J.S., Baldan, M.R.: Production and characterization of activated carbon fiber from textile PAN Fiber. J. Aerosp. Technol. Manag. (2017). https://doi.org/10.5028/jatm.v9i4.831
31. Arbizzani, C., Yu, Y., Xiao, J., Xia, Y., Yang, Y., Santato, C., Raccichini, R., Passerini, S.: Good practice guide for papers on supercapacitors and related hybrid capacitors for the Journal of Power Sources. J. Power Sources (2020). https://doi.org/10.1016/j.jpowsour.2019.227636
32. Balducci, A., Belanger, D., Brousse, T., Long, J.W., Sugimoto, W.: A guideline for reporting performance metrics with electrochemical capacitors: from electrode materials to full devices. J. Electrochem. Soc. (2017). https://doi.org/10.1149/2.0851707jes
33. Kurra, N., Jiang, Q.: Electrochemical characterization techniques for supercapacitors. In: Storing energy with special reference to renewable energy sources, pp. 401–403. Elsevier (2022).
34. Jinitha, C.G., Jeba, S.V., Sonia, S. Ramachandran, R.: Fundamentals of supercapacitors. In: Smart supercapacitors fundamentals, structures, and applications, pp. 85–87. Elsevier (2023).
35. Muzaffar, A., Ahamed, M.B, Hussain, C.M.: Electrolyte materials for supercapacitors. In: Smart supercapacitors fundamentals, structures, and applications, pp. 231–232. Elsevier (2023).
36. Zhang, S., Pan, N.: Supercapacitors Performance Evaluation. Adv Energy Mater (2015). https://doi.org/10.1002/aenm.201401401
37. Pandolfo, T., Ruiz, V., Sivakkumar, S., Nerkar, J.: General properties of electrochemical capacitors. In: Supercapacitors: materials, systems, and applications, pp. 70 - 71- . Wiley-VCH (2013).
38. Muzaffar, A., Ahamed, M.B., Hussain, C.M.: Testing and measurement techniques for supercapacitors. In: Smart supercapacitors fundamentals, structures, and applications, pp. 667. Elsevier (2023).
39. Jiménez, V., Sánchez, P., Romero, A.: Materials for activated carbon fiber synthesis. In: Activated carbon fiber and textiles, pp. 21–38. Woodhead Publishing Series in Textiles (2017).
40. Zhang, X.H., Li, Q.W.: Carbon fiber spinning. In: Activated carbon fiber and textiles, pp. 39–60. Woodhead Publishing Series in Textiles (2017).

41. Yue, Z., Economy, J.: Carbonization process – Carbonization and activation for production of activated carbon fibers. In: Activated carbon fiber and textiles, pp. 78. Woodhead Publishing Series in Textiles (2017).
42. Yue, Z., Economy, J.: Activation process – Carbonization and activation for production of activated carbon fibers. In: Activated carbon fiber and textiles, pp. 85–86. Woodhead Publishing Series in Textiles (2017).
43. Yue, Z., Economy, J.: Development of porosity – Carbonization and activation for production of activated carbon fibers. In: Activated carbon fiber and textiles, pp. 89–94. Woodhead Publishing Series in Textiles (2017).
44. Donohue, M.D., Aranovich, G.L.: Classification of Gibbs adsorption isotherms. Adv. Coll. Interface. Sci. **76–77**, 137–152 (1998)
45. Chang, S.S., Clair, B., Ruelle, J., Beauchêne, J., Renzo, J.D., Quignard, F., Zhao, G.J., Yamamoto, H., Gril, J.: Mesoporosity as a new parameter for understanding tension stress generation in trees. J. Exp. Bot. (2009). https://doi.org/10.1093/jxb/erp133
46. Gleysteen, L.F., Deitz, V.R.: Hysteresis I the physical adsorption of nitrogen on bone char and other adsorbents. J. Res. Natl. Bur. Stand. **35**, 285–307 (1945)
47. Lahrar, H.E., Simon, P., Merlet, C.: Carbon-carbon supercapacitors: Beyond the average pore size or how electrolyte confinement and inaccessible pores affect the capacitance. J Chem Phys (2021). https://hal.science/hal-03388764.
48. Kurzweil, P.: Pore Geometry – electrochemical double-layer capacitors. In: Electrochemical energy storage for renewable sources and grid balancing, pp. 352. Elsevier (2015).
49. Scibioh, M.A., Viswanathan, B.: Electric double-layer in supercapacitors – fundamentals and energy storage mechanisms - overview. In: Materials for supercapacitor applications, pp. 27–29. Elsevier (2020).
50. Kurzweil, P.: Diffusion impedance–electrochemical double-layer capacitors. In: Electrochemical energy storage for renewable sources and grid balancing, pp. 357. Elsevier (2015).
51. Chen, J.Y.: ACF/CF structures and properties – Introduction. In: Activated carbon fiber and textiles, pp. 9–11. Woodhead Publishing Series in Textiles (2017).
52. Yue, Z., Economy, J.: Physical activation – Carbonization and activation for production of activated carbon fibers. In: Activated carbon fiber and textiles, pp. 86. Woodhead Publishing Series in Textiles (2017).
53. Farnsworth, A., Chirima, G., Yu, F.: Raman spectroscopy: a key technique in investigating carbon-based materials. Spectroscopy Online. https://www.spectroscopyonline.com/view/raman-spectroscopy-a-key-technique-in-investigating-carbon-based-materials (2021). Accessed 30 April 2020.
54. Barzegar, F., Momodu, D.Y., Fashedemi, O.O., Bello, A., Dangbegnon, J.K., Manyala, N.: Investigation of different aqueous electrolytes on the electrochemical performance of activated the electrochemical performance of activate. R Soc Chem (2015). https://doi.org/10.1039/c5ra21962k
55. Mathis, T.S., Kurra, N., Wang, X., Pinto, D., Simon, P., Gogotsi, Y.: Energy storage data reporting in perspective-guidelines for interpreting the performance of electrochemical energy storage systems. Adv Energy Mater (2019). https://hal.science/hal-02519795.
56. Castro-Gutiérrez, J., Celzard, A., Fierro, V.: Energy storage in supercapacitors: focus on tannin-derived carbon electrodes. Front. Mater. (2020). https://doi.org/10.3389/fmats.2020.00217
57. Kurzweil, P.: Electrolyte solution – electrochemical double-layer capacitors. In: Electrochemical energy storage for renewable sources and grid balancing, pp. 372–374. Elsevier (2015).
58. Scibioh, M.A., Viswanathan, B.: Cyclic voltammetry – characterization methods for supercapacitors. In: Materials for supercapacitor applications, pp. 323–327. Elsevier (2020).
59. Scibioh, M.A., Viswanathan, B.: Pseudocapacitance – fundamentals and energy storage mechanisms - overview. In: Materials for supercapacitor applications, pp. 29–30. Elsevier (2020).
60. Taberna, P.L., Simon, P.: Electrochemical impedance spectroscopy – most used electrochemical techniques. In: Supercapacitor – materials, systems, and applications, pp. 119–123. Wiley - VCH (2013).
61. Wang, Y., Song, Y., Xia, Y.: Electrochemical capacitor: mechanism, materials, systems, characterization, and applications. Chem. Soc. Rev. (2016). https://doi.org/10.1039/c5cs00580a
62. Taberna, P.L., Simon, P.: Supercapacitor impedance - electrochemical techniques. In: Supercapacitor – materials, systems, and applications, pp. 124–129. Wiley - VCH (2013).
63. Pal, B., Yang, S., Ramesh, S., Thangadurai, V., Jose, R.: Electrolyte selection for supercapacitive devices: a critical review. Nanoscale Adv. (2019). https://doi.org/10.1039/c9na00374f
64. Scibioh, M.A., Viswanathan, B.: Electrochemical impedance spectroscopy – characterization methods for supercapacitors. In: Materials for supercapacitor applications, pp. 330–336. Elsevier (2020).
65. Farma, R., Deraman, M., Awitdrus, Talib, I.A., Omar, R., Manjunatha, J.G., Ishak, M.M., Basri, N.H., Dolah, B.N.M.: Physical and electrochemical properties of supercapacitor electrodes derived from carbon nanotube and biomass carbon. Int. J. Electrochem. Sci. **8**, 257–273 (2013)
66. Benabithe, Z.Z., Diossa, G., Castro, C.D., Quintana, G.: Activated Carbon Bio-Xerogels as Electrodes for Super Capacitors Applications. Procedia Engineering (2016). https://doi.org/10.1016/j.proeng.2016.06.470
67. Gomes, J.F., Gasparotto, L.H.S., Tremiliosi-Filho, G.: Glycerol electro-oxidation over glassy-carbon-supported Au nanoparticles: direct influence of the carbon support on the electrode catalytic activity. Phys. Chem. Chem. Phys. (2013). https://doi.org/10.1039/c3cp50280e

Authors and Affiliations

Ingrid Ariani Belineli Barbosa[1] · Jossano Saldanha Marcuzzo[2] · Ivana Conte Cosentino[1] · Rubens Nunes de Faria Jr[1]

✉ Ingrid Ariani Belineli Barbosa
ingridbelineli@usp.br

[1] Nuclear and Energy Research Institute (IPEN), University of São Paulo (USP). Ave. Lineu Prestes, 2242 Cidade Universitária, São Paulo, SP CEP 05508-000, Brazil

[2] JMHP Carbon. Rua Glauber Rocha, 187 Villa Branca, Jacareí, SP CEP 12301-600, Brazil